NURETH14-101

VERIFICATION AND VALIDATION OF NUMERICAL MODELS OF THE TRANSPORT OF INSULATION DEBRIS

G. M. Cartland Glover¹, A. Kratzsch², E. Krepper¹, S. Renger², A. Seeliger², F. Zacharias², S. Alt², W. Kästner², H. Kryk¹ and F.-P. Weiss¹

¹ Helmholtz-Zentrum Dresden-Rossendorf, Institute of Safety Research, P.O. Box 510119, D-01314, Dresden, Germany

Abstract

Mineral wool fibre agglomerates (MWFA), which are released by damage to insulation materials located near to a primary circuit coolant leak, maybe transported to the containment sump strainers, where they can accumulate and compromise the long-term operation of the emergency core cooling system. Numerical models of the transport of MWFA are validated against single effect tests of sedimentation in a quiescent rectangular column and sedimentation in a horizontal flow. MWFA can be modelled as a number of pseudocontinuous dispersed phases of spherical wetted agglomerates. Agglomerate size, density, relative viscosity of the fluid-fibre mixture and the turbulent dispersion influence MWFA transport.

Introduction

Damage to insulation materials located near to a primary circuit coolant leak may compromise the operation of the emergency core cooling system (ECCS). Insulation material in the form of mineral wool fibre agglomerates (MWFA) maybe transported to the containment sump strainers, where they may block or penetrate the strainers [1]-[5]. The impact of MWFA on the pressure drop across the strainers is considered acceptable; however, the corrosion products that form over time in the containment sump may also accumulate at the blocked strainers. This may result in significantly large pressure drops across the strainers, which can cause cavitation in the ECCS. Thus, ECCS flow to the reactor vessel could become compromised.

1. Project overview

An experimental and theoretical study performed by the Helmholtz-Zentrum Dresden-Rossendorf and the Hochschule Zittau/Görlitz is investigating phenomena that maybe observed in the ECCS during a primary circuit coolant leak [6]. The study entails the generation of fibre agglomerates, the determination of their transport properties in single and multi-effect experiments and the investigation of the long-term effect that the corrosion of the containment internals by the coolant has on the observed strainer pressure drops.

² Hochschule Zittau/Görlitz, Institute of Process Technology, Process Automation and Measuring Technology, P.O. Box 1455, D-02754, Zittau, Germany

1.1 Modelling the transport of mineral wool fibre debris

The focus of this paper is on the verification and validation of numerical models that can predict the transport of MWFA to where they accumulate at the sump strainers. A number of pseudo-continuous dispersed phases of spherical wetted agglomerates represent the MWFA. The size, density, the relative viscosity of the fluid-fibre agglomerate mixture and the turbulent dispersion may affect how the fibre agglomerates are transported. In the cases described here, the size is kept constant while the density is modified. This definition affects both the terminal velocity and volume fraction of the dispersed phases. Note that the relative viscosity is only significant at high concentrations.

Three single effect experiments were used to provide validation data on the transport of the fibre agglomerates under conditions of sedimentation in a quiescent fluid, sedimentation in a horizontal flow and suspension in a horizontal flow. The experiments were performed in a rectangular column for the quiescent fluid and a racetrack type channel that provided a near uniform horizontal flow. The numerical models of sedimentation in the column and the racetrack channel found that the sedimentation characteristics are consistent with the experiments. For the suspension or transport of the MWFA in the channel, the heavier MWFA tend to accumulate at the channel base even at high velocities, while lighter MFWA are more likely to be transported around the channel [7]. Further experiments are currently being performed and analysed on the suspension of the MFWA in order to provide CFD quality data for the validation of the appropriate simulations. Thus, the suspension experiments and simulations will not be discussed here.

1.2 Modelling techniques

The modelling of the flow phenomena in the containment sump during a LOCA has previously been considered in a single-phase reference frame in combination with probabilistic risk assessments to determine the extent of fibre deposition at the sump strainers [4], [8]-[10]. However, this introduces significant uncertainties into the assessment of the quantity of debris that may reach and penetrate the sump strainers. Therefore, various approaches are being developed to resolve the transport of the debris via the application of two or three-dimensional multiphase flow models in order to reduce such uncertainties [6]-[7], [11].

Various methods can be used to model the transport of particles that differ in complexity and computational intensity. The modelling methods include discrete element methods [12]-[13], discrete particle tracking [14]-[15] and dispersed pseudo-continuum phase models [16]. The complexity is characterized by the way in which the motion of the particles is described. For example, the discrete element methods resolve the short and long-range forces acting on spherical particles, while for flexible fibres the stresses within the fibres are also resolved. For discrete particle tracking, a balance of interfacial forces is used to estimate the displacement of the particles by particle collisions and fluid motion. Both of these methods would require significant computational intensity to resolve the large number of particles present in the flows examined here. The pseudo-continuous phase approach simplifies the

modelling of the particles by determining the probability of the presence of particles via a "volume fraction equation", where the two-fluid or drift flux modelling approaches are considered when applying pseudo-continuous phases. The key difference between the two approaches is the number of mass and momentum continuity equations that are used. The advantage of such approaches is that larger, more complex domains can be considered along with higher concentrations. However, the phase description is limited to either a single typical dispersed phase or only a few dispersed phases due to the additional computational load involved.

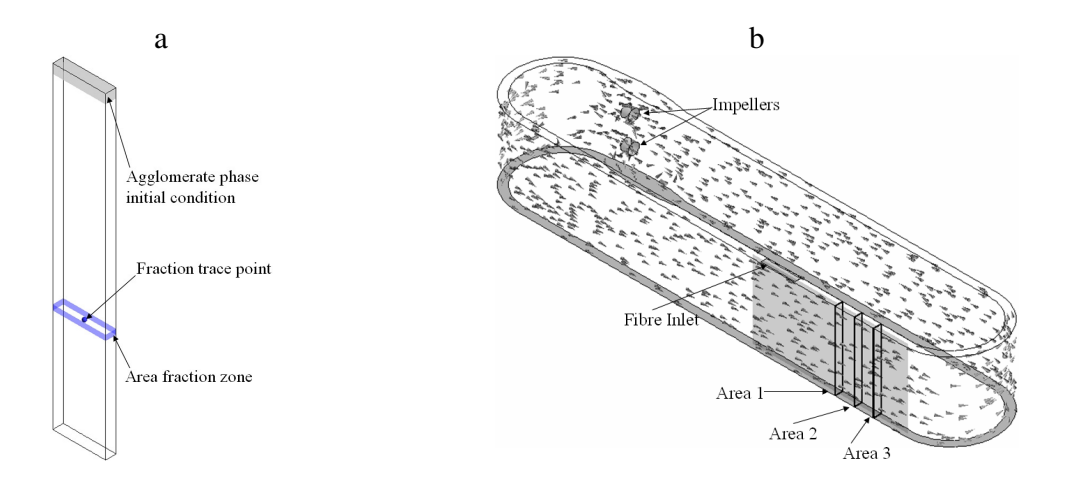


Figure 1 Images of the vertical column and the racetrack type channel.

2. Experimental facilities

2.1 Configurations

Two experimental facilities (Figure 1) were used to characterise the sedimentation characteristics of the MWFA. A 3 m high by 1 m wide Plexiglas column with a thickness of 10 cm was used to observe sedimentation in a quiescent column, while a racetrack type channel was used to observe sedimentation in a cross flow. The channel has a width of 0.1 m and a depth of 1.2m. The length of the straight sections is 5 m, while the bends have a radius of 0.5 m. The water flow is driven by two slow moving impellers (Type: EMU TR 14.145-4/6, WILO EMU GmbH) that drive the liquid at velocities of between 0.01 and 0.6 m s⁻¹. Note that the channel is expanded to 0.2 m in order to accommodate the pumps. The walls are constructed from 30 mm thick Plexiglas.

2.2 Measurement techniques

The motion of the particles through the column and the channel were observed through particle imaging techniques. This was achieved by using low-speed 8-bit greyscale CMOS cameras (MC1301 camera of Mikrotron GmbH) with a resolution of 1280 by 1024 Pixels at a frame rate up to 100 frames per second. The unmagnified pixel size of the cameras is 12 µm

by $12 \mu m$. Two cameras were trained on the top and bottom halves of the vertical column and on the two segments that were below and downstream of the drop tray in the channel, as indicated in Figure 1b. Data was extracted via means of estimating the particle area fraction observed within a specific region or the greyscale profile across the column width or the channel height.

The key uncertainty in the particle imaging performed here is that there maybe some variation of the MWFA distribution over the width of the measurement regions (0.1 m), as some agglomerates could obscure other agglomerates. The particle imaging in its current form cannot estimate the volumetric extent of the particles, as the cameras have not been used stereoscopically. Therefore, direct comparisons of the experimental data with the volume fraction distributions obtained from three-dimensional flow simulations may miss a portion of the volume of fibre agglomerates. Note that at the magnification used the particle imaging was not able to capture the motion of individual fibres in the channel.

2.3 Experimental schemes

Drop trays were used to insert a known quantity of wetted MWFA at a specific location. The quantity of fibre agglomerates in both the channel and column was 21.9 g of dry MWFA that had been steam blasted. This mass of MWFA was then wetted in 1 l of water and dropped into the column or the channel from the drop trays. These trays were located at the top of the column and 3.14 m from the end of the first bend after the impellers. The channel drop tray was 0.44 m long and located a short distance above the surface of the liquid.

The impellers were operated at frequency that gave a mean velocity of 0.2 m s⁻¹ when the impellers were positioned at heights of 0.305 m and 0.68 m in the expanded section (Figure 1b). The particle imaging was left to run for the time it took for the majority of fibre agglomerates to pass through the field of view. This was 300 s for the column sedimentation and around 10 s for the channel sedimentation.

3. Numerical models

3.1 Hydrodynamic models

A two-fluid model (TFM) is used in combination with the drift flux model (DFM) to determine the transport of a number of dispersed phases and is herewith indicated by the abbreviation TFM-DFM (Figure 2). Both the two-fluid and the drift flux models are standard models in the solver ANSYS CFX [17], where the transport equations are indicated in Figure 2.

The drift flux model considers the dispersed phases as a mixture through N_q mass fraction equations and one set of mass and momentum conservation equations, where the phase interactions are determined by a drift velocity. The two-fluid model is resolved by a full set of mass and momentum conservation equations for both the dispersed and continuous phases

along with a conservation equation of the volume fraction for the dispersed phase. Momentum exchange terms are used to determine the interactions between the phases caused by particle drag.

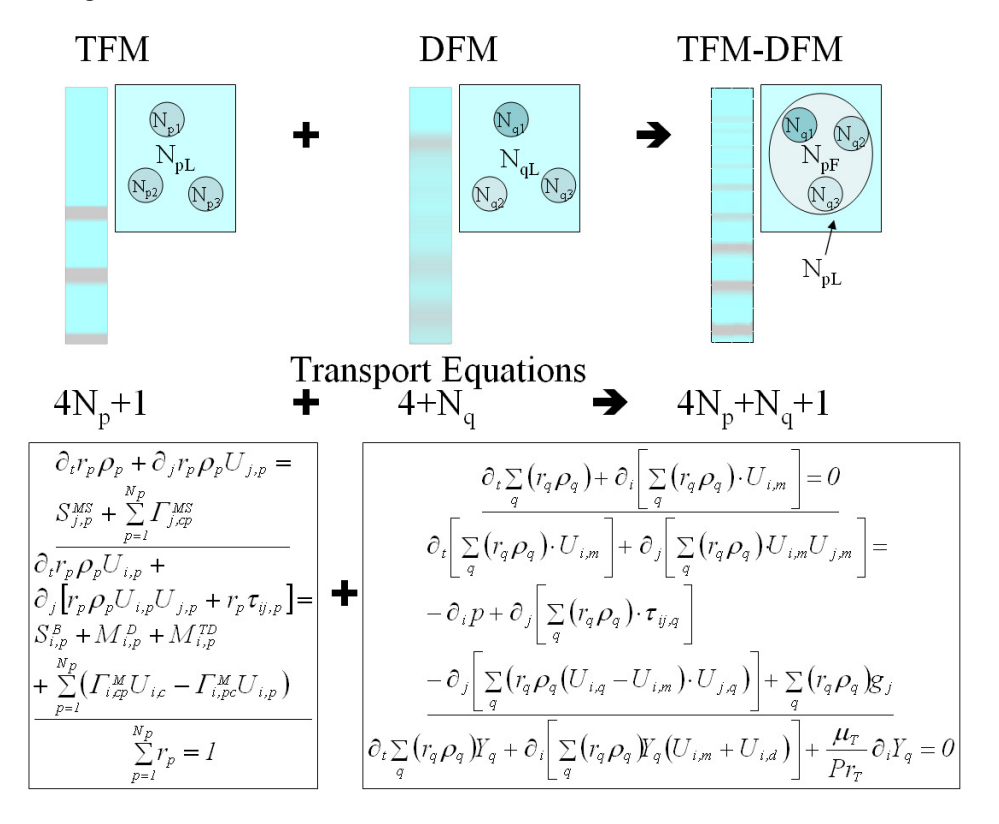


Figure 2 The contours of volume fraction from equivalent simulations of column sedimentation, morphology and transport equations for the two-fluid (TFM) and drift flux (DFM) models. The equations of continuity of mass, momentum and phase fraction are indicated in the left box for the two-fluid model and the right box for the drift flux model. All parameters and variables in this figure are defined in the nomenclature.

3.2 Interfacial forces

In the two-fluid model the buoyancy force, the drag force and the turbulence dispersion force are the only forces that are considered as significant, while the lift, wall lubrication and the virtual mass forces are assumed to have a negligible effect on the fibres. The solids particle collision models and any agglomeration, erosion or breakage of the MWFA is not accounted for in the current model. Such models require detailed empirical knowledge of the individual fibre and agglomerate behaviour.

In the simulations described here, the turbulence dispersion coefficient of the Eulerian dispersed phase is a constant with a value of 1. For the mixture phases, the form of the turbulence dispersion force is based on the multi-component diffusion term, which does not account for the effect of particle drag on the dispersion of the particles. The modelled MWFA

are assumed to have the form of wetted spherical particles with a constant diameter. The drag coefficients for all dispersed phases were estimated using the Schiller-Naumann correlation.

3.3 Turbulence model

The turbulence model used here was the standard implementation of SST or Shear Stress Turbulence transport model of ANSYS CFX [17], The SST model was applied to the continuous phase with automatic wall functions. Simulations applying different turbulence models to a section of the channel showed that k- ω type turbulence models applied with automatic wall functions could adequately model the flow in the near-wall region. The turbulent viscosity of the Eulerian dispersed phase is resolved through the use of the zero-equation model, where there is an assumed proportionality to the turbulent viscosity of the continuous phase.

3.4 Case specifications

3.4.1 Phase definitions

Ten dispersed phases were defined according to the terminal velocities observed in the column sedimentation experiments, which ranged between 0.5 mm s⁻¹ for individual fibres and small clusters of fibres up to 150 mm s⁻¹ for the larger agglomerates (Figure 5b). The settling velocities, $u_{s,q}$, of the ten dispersed phases are found in Table 1. The virtual particle diameter, d_F , was selected such that the volume of all agglomerates was less than the volume in which the fibres were wetted prior to their addition to the channel, which for the simulations described here was 2.5 mm. The density, ρ_F , of MWFA could then be determined using the settling velocity and virtual particle diameter in an iterative process. Note that the share of fibres in MWFA indicates that the majority of the wetted agglomerate mass is water [6]. The viscosity of the mixture is based on the product of the continuous phase viscosity and the relative viscosity, μ_F , which was given by the correlation of Batchelor [18]:

$$\mu_r = I + 2.5r_p + 7.6r_p^2 \tag{1}$$

3.4.2 <u>Initial and boundary conditions</u>

The column was a closed rectangular grid 3 m high by 1 m wide by 0.1 m thick, it contained 88929 nodes or 76800 cubic elements with a node spacing of 0.0125 m. The wall conditions were specified with the no-slip condition.

The whole channel simulation has a mesh with 812036 nodes, which represents the impellers by using two cylindrical sub-domains (diameter of 0.14 m and length 0.1 m) [7]. The sub-domains are used to apply momentum sources with a value of 1290 kg m⁻² s⁻², This value was estimated from the head loss over the channel length via the Darcy-Weisbach equation [19] to give a mean velocity of ~0.2 m s⁻¹. Note that cylindrical walls were applied to the sub-domains to try to improve the convergence of the flow solutions.

The mass of dry fibres, m_F added to the simulations was 95% of the experimental mass, as the remainder were free fibres or small clusters with very slow settling velocities that took more time to sediment than the measurement time of the experiment. Note that the fibre material is based on steam-blasted MDK, ~5% of which had a terminal settling velocity of ~0.5 mm s⁻¹.

To define the fraction of each phase dropped in either the column or the channel for the TFM-DFM cases, a mass fraction must be defined for mixture phases 1 to 9 and volume fraction for the Eulerian dispersed phase. The tenth phase is treated as a constraint condition. The mass fractions for both the column and the channel, Y_p , were estimated for each dispersed phase using Equation (2), by taking the values of the area fraction, $\chi_{q,exp}$, from the experimental profile plotted in Figure 5b. Note that a comparative mixture model case was also performed, where 10 dispersed phases were modelled with the liquid phase applied as the constraint condition. The initial conditions for this case are given in the fourth column of Table 1.

Table 1 Definition of the MDK phases for the column sedimentation simulations, where is increased by $u_{s,a+1} = u_{s,a}^{0.92}$.

р	$U_{s,q}$	$ ho_q$	Column		Channel		$X_{q,exp}$
	(mm s ⁻¹)	(kg m ⁻³)	$10^3 * Y_q$	r_q	$10^{3}Y_{q}$	r_q	(-)
			(-)	(-)	(-)	(-)	
1	10	1003.48	0.20	0.030	0.98	0.150	0.047
2	14	1007.97	0.09	0.008	0.44	0.040	0.021
3	20	1015.05	0.09	0.005	0.44	0.024	0.021
4	28	1025.80	0.12	0.004	0.59	0.020	0.028
5	37	1041.65	0.26	0.006	1.31	0.029	0.063
6	48	1064.20	0.35	0.005	1.74	0.026	0.084
7	61	1095.30	0.82	0.008	4.07	0.041	0.197
8	77	1136.96	0.98	0.007	4.90	0.035	0.237
9	94	1191.25	0.94	0.005	4.69	0.024	0.228
10	114	1260.15	0.30	0.001	1.49	0.006	0.072
Sum	-	-	4.14	0.079	20.65	0.397	1.000

$$Y_q = \frac{\chi_{q,exp} m_F}{m_F + V \rho_L} \tag{2}$$

The volume fraction, r_p , for the Eulerian dispersed phase was estimated from the mass of MWFA added to the channel using Equation (3), where V is the volume of the drop tray and ρ_L is the liquid phase density. The values of the individual and the sum of the volume fractions are given in the fifth and seventh columns of Table 1.

$$r_{p} = \sum_{q=0}^{N_{q}} \chi_{q,exp} m_{F} (\rho_{q} - \rho_{L}) V^{-1}$$
(3)

The volume fraction applied to the initial condition for the column took the form of a location (\vec{x}) dependent step function. The inlet condition for the channel was specified as a time, t, dependent step function that corresponded to the time for the drop tray volume to enter the

channel at the inlet velocities, u_j , given in Table 2 and the corresponding volume fractions are defined in bold in the sum row of Table 1. The functions are given in Equation (4). The initial velocity condition for the column was a zero velocity condition, while the channel was initialised by an interpolated single-phase flow solution.

$$Column: Channel: Y = r_p = 0 \quad \vec{x}_{min} > \vec{x} \quad \vec{u} = (0, u_{in,j}, 0) \quad 0 < t < t_{in,max}$$

$$Y = Y_q \quad \vec{x}_{min} < \vec{x} < \vec{x}_{max} \quad Y = Y_q \quad 0 < t < t_{in,max}$$

$$r_p = \sum_q r_q \quad \vec{x}_{min} < \vec{x} < \vec{x}_{max} \quad r_p = \sum_q r_q \quad 0 < t < t_{in,max}$$

$$Y = r = 0 \quad \vec{x} > \vec{x}_{max} \quad \vec{u} = Y = r = 0 \quad t > t_{in,max}$$

$$Y = r = 0 \quad \vec{x} > \vec{x}_{max} \quad \vec{u} = Y = r = 0 \quad t > t_{in,max}$$

Table 2 Definition of the time dependent inlet conditions and the number of dispersed phases.

Sim.	А	В	С	D	Е	E-TFM-DFM
$t_{in,max}$ (s)	0.0150	0.0275	0.0325	0.0450	0.0650	0.0650
$u_{in,j}$ (m s ⁻¹)	2.083	1.052	0.897	0.662	0.481	0.481
$N_p + N_q$	1	1	1	1	1	10

The velocity at the fibre inlet, as located in §2.3, was estimated assuming a perfectly inelastic collision with the fibre volume fraction given in the last row of the seventh column of Table 1. It was assumed that the fibre water mix dropped approximately 20 cm. The injection period was varied with the injection velocity, as indicated in Table 2, in order to match the behaviour of the MFWA observed at the start of the experiments. Note that the dispersed phase was defined such that for cases A to E $u_{s,p} \approx 50$ mm s⁻¹, $d_p = 5$ mm and $\rho_p = 1027$ kg m⁻³. The remaining conditions are no-slip walls applied to the base and sidewalls of the channel and a free-slip condition is applied to the top surface for the single-phase case. The top surface conditions are defined as a zero-velocity inlet condition with a zero-gradient turbulence condition for the multiphase calculations. Three 20 mm wide analysis regions (Areas 1 to 3 in Figure 1b) are positioned downstream of the inlet condition beginning at 4.0995, 4.34825 and 4.597 m from the end of the first bend after the impellers.

3.4.3 <u>Grid resolution at the wall</u>

The resolution of the grid in the boundary layer is significant as the channel width is small. The maximum y^+ value for the channel simulation is 177 on false impeller walls. While the maximum y^+ value on the remaining walls is 34, which indicates that the mesh is adequately resolved near to the wall for the suspension section and whole channel simulations for sedimentation when the SST model is applied with automatic wall functions. The y^+ values were between 1 and 13 for the DFM cases and between 1 and 100 for the TFM-DFM cases for the duration of the sedimentation.

3.5 Solution techniques

The solution techniques applied to all simulations included the definition of the initial static pressure as $g_j * \rho_L * h$ and the use of the high-resolution mode of the solver for the advection and turbulence numerics schemes [17]. Note that h is the vertical distance, g_j is the acceleration due to gravity. Segregated volume fraction equations and volume-weighted body forces were used when TFM was applied [17]. Time was advanced with the second order backward Euler scheme [17].

The column simulations were performed over a period of 300s, where the time step size was varied between 0.001 s and 0.01 s for the TFM-DFM simulations and between 0.005 s and 0.1 s for the DFM cases.

The single-phase transient step resolved the transport of water through the channel for 400 s or approximately 5 circuits of the channel. The flow field was initialised on a coarse version of the mesh (367372 nodes) with zero velocity conditions and automatically defined turbulence parameters. After 150 s, the flow field from the coarse mesh was used to initialise the case with the final mesh by interpolation. Each time step was considered converged when the maximum residuals of the momentum equations were less than 10^{-4} . Note that adaptive time stepping was used to increase the time-step size from 0.005 s to 0.05 s during the course of the single-phase simulation. The largest time step size used gave a maximum Courant number of 7.

The dispersed phase transient step modelled the transport of a slug of fibre agglomerates from the inlet for 10 s. Two time step sizes were used with 0.0025 s for the first 0.499 s and 0.005 s for the remainder of the simulation. Each time step was considered converged when the root mean square residuals of the momentum and mass fraction equations were less than $2*10^{-4}$. The maximum Courant number was of the order of 1 throughout the simulation.

4. Results

4.1 Column sedimentation

Traces from the experimental and numerical studies of sedimentation in a quiescent column are found in Figures 3-5. Figure 3 verifies the application of the combined TFM-DFM model to the settling of MWFA. It shows a comparison with the expected and the calculated settling velocity as the simulation progresses at a point 2 m below the top of the column.

Note that in Table 1, phase 10 was defined as a constraint phase with an expected settling velocity of 114 mm s⁻¹. This meant that this phase is not explicitly modelled with a drift flux equation. Thus, the largest velocity, which is in effect modelled, corresponds to the ninth phase given in Table 1. This can be observed by the absence of the simulated velocity around the first data point on the theoretical curve.

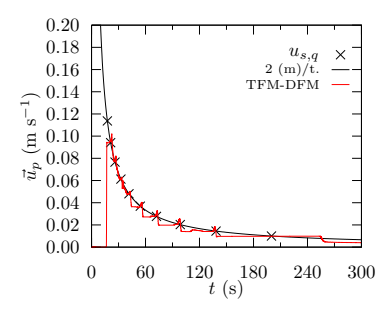
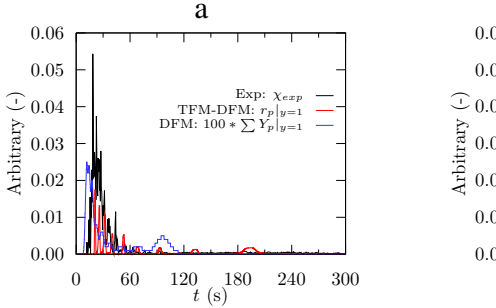


Figure 3 Trace of the MWFA settling velocity for MDK in the quiescent column, where the specified values of $u_{s,q}$ are indicated to aid comparison.

Three traces located 2m below (Figure 1a) the drop tray are shown in each plot of Figure 4, one for the experimental area fraction, as determined by Equation (5) and two point traces. The traces obtained from the full DFM and the combined TFM-DFM simulations were respectively specified as point traces of the overall mass fraction and the overall volume fraction for all of the dispersed phases. Note that $N_{ax,F}$ is the number of pixels in the measurement area occupied by MWFA and N_{max} is the total number of pixels in the measurement zone.

$$\chi_{exp} = N_{x,F} / N_{max} \tag{5}$$

The traces in Figure 4 show that both models can replicate the typical distributions observed in the experiments, though the full DFM approach tends to over-predict the settling velocity for the heavier dispersed phases. The largest specified velocity is somewhat lower than the largest settling velocities observed in the experiments, as the intention was to model steamblasted MD2 with the same settling velocity distribution as well. However, due to space limitations, the traces for MD2 are not reported here.



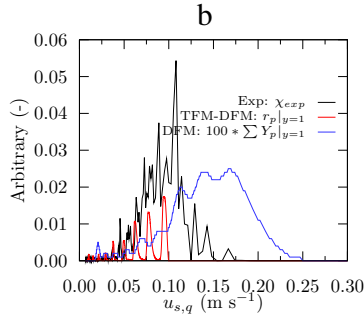


Figure 4 Traces of column sedimentation of MDK. a) Traces based on Equation (5) and point values versus time; b) Traces from Figure 4 a) versus settling velocity;

Nevertheless, it is difficult to compare directly the values of the point traces of the volume fraction against the area fractions. Therefore, normalised cumulative sums of all of the traces were made to aid the comparison of the different traces. These traces are depicted in Figure 5. The traces show that the combined TFM-DFM model offers a significant improvement in the modelling of the sedimentation of MWFA. This can be seen in the trends of both plots in

Figure 5, where the traces for the TFM-DFM simulations are similar to the experimental traces.

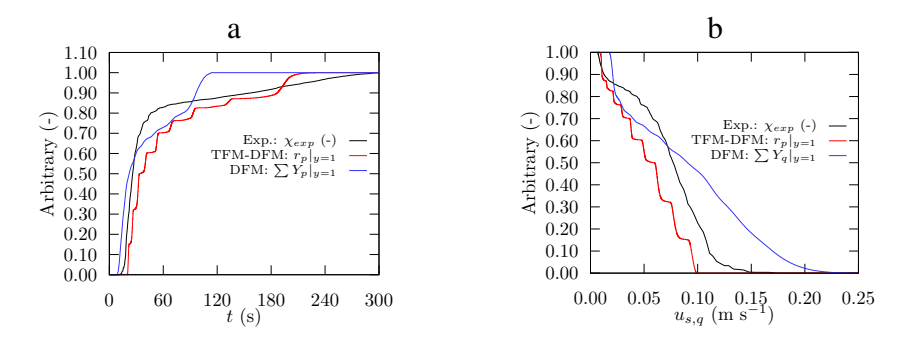


Figure 5 Normalised cumulative sum of traces obtained from column sedimentation of MDK. a) Traces obtained from Figure 4 a) versus time; b) Traces from Figure 5 a) versus settling velocity;

4.2 Channel sedimentation

Traces and the time evolution of profiles from the experiments and the simulations of sedimentation in the channel are presented in Figures 6 and 7. The traces in Figure 6 depict the change in the area or volume fraction of the MWFA dispersed phase, as it is passes through the third measurement area (Figure 1b). Note that χ is determined from Equation (6) for the simulated data, where V is the volume and the subscripts have a similar meaning as in Equation (5).

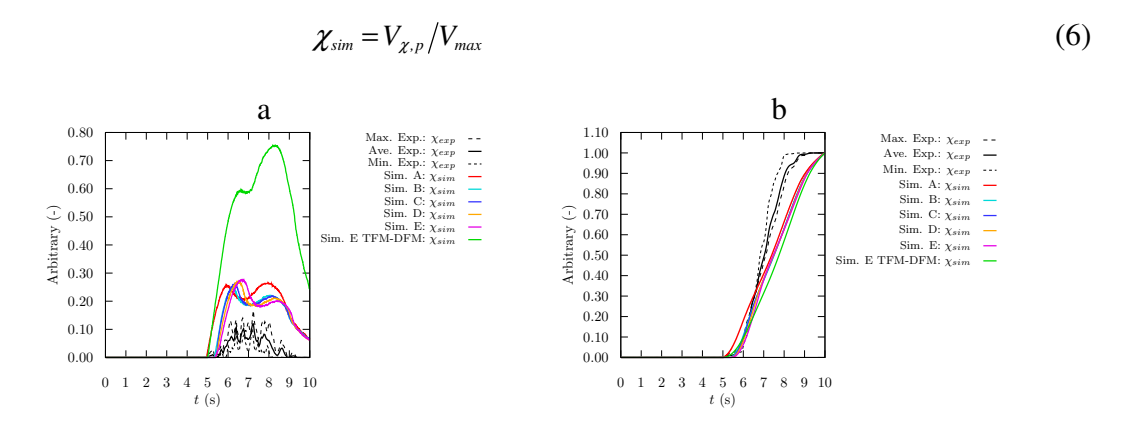


Figure 6 Channel traces obtained from Area 3. a) Traces based on Equations (5) and (6); b)

Normalized cumulative sum of the traces;

The comparison of the traces derived from Equations (5) and (6) is not like for like, as the fraction obtained from the experiments is based on the area occupied by MWFA on a midplane focal length, while the volume fraction is taken over the whole width of the channel. Therefore, two forms of traces are presented in the same way as for the column traces, where the "raw" trace data are plotted in Figure 6a and the normalised cumulative sum of the traces

are found in Figure 6b. The traces show the influence that the injection velocity has on the initial form of the curve; however, dispersion effects and the nature of the quantities measured show their influence in both plots. All the simulations differ from the experiments in that tails form in the dispersed phase slug, which manifests itself in the different gradients of the curves of Figure 6b, and the time lag at the end of the curves of Figure 6a. The tails form due to the influence of the velocity profile observed over the channel width, which in turn influences the eddy viscosity and therefore the turbulent dispersion force. Note that the tails are not seen the experiments.

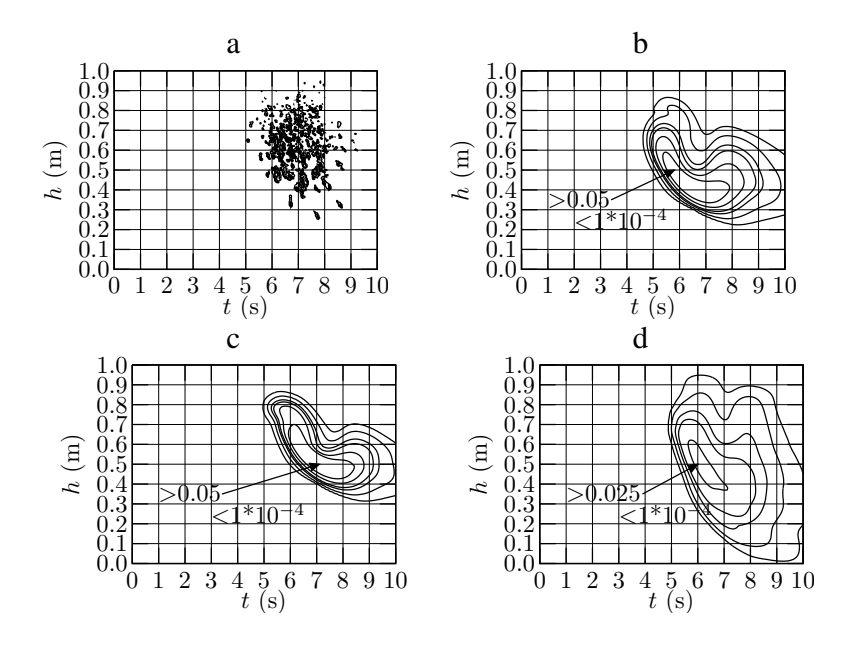


Figure 7 Sequential channel profiles from Area 3. a) Averaged experimental profiles; b) Sim. A; c) Sim. E; d) Sim. E TFM-DFM;

The time evolution of the profiles from the experiment in Figure 7a show that the larger heavier agglomerates drop more than 0.5 m over the distance they are observed, while the lighter agglomerates remain in the top half of the channel and some of the lightest agglomerates do not descend lower than 10 cm under the free surface. For cases Sim A to Sim E, the change in the inlet velocity has a marginal influence on how far the MFWA phase sediments over the two segments. For Sim A (Figure 7b), the lowest height of the region of the 0.05 fraction contour is found between 0.3 and 0.4 m, while this occurs between 0.4 and 0.5 m for Sim E (Figure 7c). It could be said that the Sim E conditions give the dispersion that is closest to reality for simulations, where only a single dispersed phase is used.

In the case of Sim E TFM-DFM (Figure 7d) when ten dispersed phases are considered, the distribution of the phases spreads over the majority of the channel height. The distribution is more representative of the experimental behaviour, as more of the lighter MFWA remains in the top half of the channel, which important in regard to the transport of MWFA to the strainers. Thus, the behaviour of the dispersed phases in the model developed here is verified and partially validated against detailed experimental data. However, further improvements to

the model can be made by considering alternative turbulence models, refined meshes, different phase definitions and closure models. Nevertheless, locally refined grids have shown little effect on the shape and motion of the injected MWFA [7].

5. Conclusions

The simulations and experiments described here show the attempts made to verify and validate the assumptions made in modelling the sedimentation of mineral wool fibre agglomerates (MWFA). The experiments and simulations performed were sedimentation in a quiescent column and sedimentation in a horizontal flow generated in a racetrack type channel. A multiple dispersed phase configuration that was a combination of the two-fluid and the drift flux modelling approaches showed that the inclusion of more phases could improve the characterisation of the transport of MWFA. However, the velocity profiles near to the vertical walls and the turbulence parameters have a strong influence on the dispersion of the MWFA in the channel in the form of tails near to the wall.

6. Nomenclature

CFD computational fluid dynamics

DFM drift flux model

ECCS emergency core cooling system

LOCA loss of coolant accident

MWFA mineral wool fibre agglomerates

TFM two-fluid model

TFM-DFM combined two-fluid and drift flux model

Latin Symbols

d	(m)	diameter
g	$(m s^{-2})$	acceleration due to gravity
h	(m)	vertical distance
k	$(m^2 s^{-2})$	turbulent kinetic energy
M	$(kg m^{-2} s^{-2})$	momentum source term
m	(kg)	mass
N	(-)	number
p	(kg m2 s-2)	pressure
r	(-)	volume fraction
S	(kg m2 s-2)	mass source term
t	(s)	time
U	$(m s^{-1})$	simulated velocity
и	$(m s^{-1})$	velocity
V	(m^3)	volume
\vec{x}	(m)	location vector
Y	(-)	mass fraction
y^+	(-)	Non-dimensional distance to the wall of the first node

Greek Symbols

Γ	$(kg m^3 s^{-1})$	interphase exchange term
μ_r	(-)	relative viscosity
μ_T	$(kg m^{-1} s^{-1})$	turbulent or eddy viscosity
ρ	$(kg m^{-3})$	density
τ	$(kg m^{-2} s^{-2})$	stress tensor
χ	(-)	area, pixel or volume fraction
ω	(s^{-1})	turbulent eddy frequency

Superscripts and Subscripts

В	buoyancy
D	drag

c continuous or cth phase

d drift

exp experiment
F fibre phase
i ith direction

in inlet

j jth direction L liquid phase M momentum

MS mass

m mixture phase (drift flux)

max maximum minimum

p pth phase (two-fluid) q qth phase (drift flux)

r relative s settling sim simulated T turbulent

TD turbulent dispersion

t time

χ fraction of MWFA

7. References

- [1] NEA, "Knowledge base for emergency core cooling system recirculation reliability", NEA/CSNI/R(95)11, 1996.
- [2] NEA, "Knowledge base for strainer clogging modifications performed in different countries since 1992", NEA/CSNI/R(2002)6, 2002.

- [3] NEA, <u>Proceedings of debris impact on emergency coolant recirculation workshop</u>, Albuquerque, NM, USA 2004 February, Proceedings OECD 2004 NEA No. 5468.
- [4] USNRC, "GSI-191: Integrated debris-transport tests in containment floor geometries", NUREG/CR-6773 LA-UR-02-6786, 2002.
- [5] USNRC, 2003. "Knowledge base for the effect of debris on pressurized water reactor emergency core cooling sump performance", NUREG/CR-6808; LA-UR-03-0880.
- [6] E. Krepper, G. Cartland-Glover, A. Grahn, F.-P. Weiss, S. Alt, R. Hampel, W. Kaestner, A. Seeliger, "Numerical and experimental investigations for insulation particle transport phenomena in water flow", *Annals of Nuclear Energy*, Vol. 35, Issue 8, 2008, pp. 1564-1579.
- [7] G. M. Cartland Glover, E. Krepper, H. Kryk, F.–P. Weiss, S. Renger, A. Seeliger, F. Zacharias, A. Kratzsch, S. Alt, and W. Kästner "Fibre agglomerate transport in a horizontal flow", <u>Proceedings of the CFD for Nuclear Reactor Safety Applications (CFD4NRS-3) Workshop</u>, Bethesda, Maryland, USA, 2010, September 14-16, Paper 10.2.
- [8] H. L. Detar, D. T. McLaughlin, R. J. Lutz, "Probabilistic Model for debris-induced loss of long term core cooling, <u>Proceedings of the 16th International Conference on Nuclear Engineering</u>, Orlando, Florida, USA, 2008 May 11-15, ICONE16-48780.
- [9] J. I. Lee, S. J. Hong, J. Kim, B. C. Lee, Y. S. Bang, D. Y. Oh, B. G. Huh, "Debris transport analysis related with GSI-191 in advanced pressurized water reactor equipped with incontainment refuelling water storage tank", <u>Proceedings of the XCDF4NRS</u>
 <u>Workshop "Experiments and CFD Code Applications to Nuclear Reactor Safety"</u>, Grenoble, France, 2008 September 10-12, AC-05.
- [10] K. M. Seo, C. H. Shin, W. T. Kim, J. P. Park, B. S. Han, "CFD Analysis on Debris Transport to the Containment Recirculation Sump for OPR1000 Plant", <u>Proceedings of the 13th International Topical Meeting on Nuclear Reactor Thermal Hydraulics</u>, Kanazawa City, Japan, 2009 September 27-October 2, N13P1141.
- [11] Y. S. Bang, G. S. Lee, S. W. Woo. "A shallow water equation solver and particle tracking method to evaluate the debris transport", <u>Proceedings of the CFD for Nuclear Reactor Safety Applications (CFD4NRS-3) Workshop</u>, Bethesda, Maryland, USA, 2010, September 14-16, Paper 10.5.
- [12] F. Geng, Y. Li, X. Wang, Z. Yuan, Y. Yan D. Luo, "Simulation of dynamic processes on flexible filamentous particles in the transverse section of a rotary dryer and its comparison with ideo-imaging experiments", *Powder Technology* Vol. 207, Issue 1-3, 2011, pp. 175-182.
- [13] A. Vakil, S. Green, "Flexible fiber motion in the flow field of a cylinder", *International. Journal of Multiphase Flow*, Vol. 37, Issue 2, 2011, pp. 173-186.
- [14] A. Soldati, 2005. "Particles turbulence interactions in boundary layers", *Zeitung für Angewandte Mathematik und Mechanik*, Vol. 85, Issue 10, 2005, pp. 683-699.

- [15] I. Vinkovic, D. Doppler, J. Lelouvetel, M. Buffat, "Direct numerical simulation of particle interaction with ejections in turbulent channel flows", *International Journal of Multiphase Flow*, Vol. 37, Issue 2, 2011, pp. 187-197.
- [16] M. Eesa, M. Barigou, "Horizontal laminar flow of coarse nearly-neutrally buoyant particles in non-Newtonian conveying fluids: CFD and PEPT experiments compared", *International Journal of Multiphase Flow*, Vol. 34, Issue 11, 2008, pp. 997-1007.
- [17] ANSYS, "ANSYS CFX-12", Ansys Inc., Canonsburg, PA, USA, 2009.
- [18] G. K. Batchelor, "The effect of Brownian motion on the bulk stress in a suspension of spherical particles", *Journal of Fluid Mechanics*, Vol. 83, Issue 1, 1977, pp. 97-117.
- [19] J. M. Coulson, J. F. Richardson, J. R. Backhurst, J. H. Harker, "Coulson & Richardson's Chemical Engineering, Volume 1, fourth edition", Pergamon Press, Oxford & New York, 1990, pp. 54, 69 & 77.